Practical Implementation of a Novel Anti-Windup Scheme in a HDD-Dual-Stage Servo-System

Guido Herrmann, *Member, IEEE*, Matthew C. Turner, *Member, IEEE*, Ian Postlethwaite, *Fellow, IEEE*, and Guoxiao Guo, *Member, IEEE*

***Abstract*—Two novel discrete anti-windup (AW) techniques are applied to a dual-stage actuator of an experimental hard disk drive system. The techniques, one low order, the other full order, employ convex l_2-performance constraints in combination with linear-matrix-inequality-optimization methods. It is shown that the AW compensators can improve the performance of the nominal dual-stage servo-system when the secondary actuator control signal saturates at its allowable design limits. Also, stability is achieved despite saturation of both the secondary actuator and the voice-coil-motor actuator. Practical results show that the performance of each AW compensator is superior to another well-known *ad-hoc* AW technique, the internal model control AW scheme. The main contribution of the paper is the application of theoretically rigorous AW methods to an industrially relevant servo system.**

***Index Terms*—Anti-windup (AW) control, coarse-fine control, discrete control, hard-disk servo-system.**

I. Introduction

ONE OF THE most important developments in hard disk drive (HDD)-technology during the last decade was the increase in data storage density. However, for future high data-density disk drives, the voice-coil motor (VCM) actuator may not be sufficient to access the concentric data tracks with the required accuracy. High-bandwidth secondary actuators mounted on the VCM-actuator have been investigated for many years [16] and are regarded as a feasible alternative [13] to single-stage servo systems (see Fig. 1). However, the displacement range of these actuators is usually less than 1–2 μm for the case of actuated suspensions and even as low as 0.2 μm for some high-bandwidth actuators [15], so that manufacturers of secondary actuators recommend a limited input signal range to protect the actuator against mechanical damage. Due to this strict constraint, secondary actuator signals usually saturate before the VCM-actuator signal, and the performance of a track following controller may become unacceptable during control-signal saturation or the servo-control system may even be driven unstable.

With particular reference to HDD-servo systems, a continuous-time output-feedback control scheme capable of dealing with actuator saturation has been recently presented in [1], and, in terms of a discrete-time state-feedback control scheme, in [30]. Both these control schemes combine a nonlinear and a linear control element of fixed structure and apply to *single* input systems such as VCM-actuators. However, in principle at least, employing results from [26], the control schemes could also be used on dual-actuator systems. Nevertheless, in this paper we prefer to use linear control techniques to design a good sampled data and discrete track following controller, since bandwidth constraints for the sensitivity response in track following controllers are very tight.

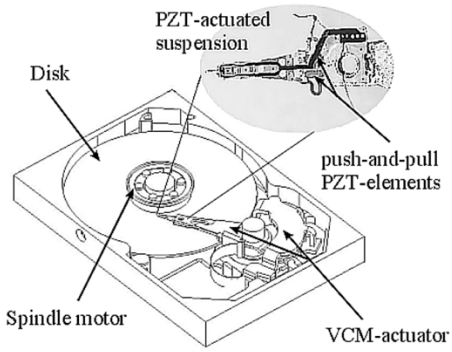

Fig. 1. Schematic of HDD with PZT-actuator.

For a dual-stage servo system, during track following and without secondary actuator saturation, the controller has to be able to compensate for the most common disturbances. This necessitates that the secondary actuator is only employed in the high-frequency region to improve the servo-control bandwidth [22] preventing saturation due to low-frequency disturbances. Hence, secondary actuator saturation should only occur during seek operations or due to large *shock disturbances*. The usual approach of dealing with the limited actuator range of the secondary actuator is to employ path planning approaches and to enable the secondary actuator controller only when the read/write head is close enough to the target track [12], [20]. For seeking new target tracks, this approach is *the preferred option*.

For severe disturbances, controller scheduling necessitates add-on sensing techniques, which allow the secondary actuator to be disabled once a disturbance occurs. Different techniques, such as extra force sensors [14], [21] or schemes using servo information from all available disk surfaces [2] for better head positioning on one surface are possible. However, even cheap force sensors can drastically increase the cost of a low-cost product such as a hard disk. Furthermore, modern HDD-products often carry only one disk using one surface only so that the scheme of [2] is not always applicable. Other alternatives for efficient disturbance detection would be to sense the head disk spacing via

Manuscript received May 4, 2003; revised August 19, 2003 and November 7, 2003. This work of G. Herrmann was funded by A*STAR Data Storage Institute, Singapore 117608, under a Senior Research Fellowship.

G. Herrmann, M. C. Turner, and I. Postlethwaite are with the Department of Engineering, University of Leicester, Leicester LE1 7RH, U.K. (e-mail: Guido_HERRMANN@ieee.org; mct6@le.ac.uk; ixp@le.ac.uk).

G. Guo is with the A*STAR Data Storage Institute, Singapore; (e-mail: GUO_Guoxiao@dsi.a-star.edu.sg.

Digital Object Identifier 10.1109/TMECH.2004.835333

the MR-head voltage [14] or to use a sufficiently fast disturbance observer [33]. Using any of these methods, switching conditions are needed to disable the secondary actuator. However, severe disturbances tend to be very short so that it can be difficult to disable the secondary actuator fast enough to prevent saturation immediately. Furthermore, any fast disabling and re-enabling of the secondary actuator may result also in severe controller action and, potentially, stability problems. This is particularly so when the switching condition is made very sensitive. Performance degradation may follow if control via the secondary actuator is resumed too late.

A different approach would be to introduce an add-on compensator which acts to retain stability and performance once the actuator signals saturates rather than sensing a disturbance to disable the secondary actuator. Hence, once the control system recovers from saturation, the linear track following design is used again. An effective engineering solution for this has been introduced recently in [8], by enlarging the region of stability and improving performance for the saturated secondary actuator.

An alternative and practically appealing way of approaching this is through anti-windup (AW) compensation where an add-on compensator is introduced to retain stability and performance in the face of actuator saturation. AW compensators, traditionally used to counter integrator windup, (see [19] for an example), have received significant attention during recent years [4], [5], [7], [24] and a number of techniques are now available for the synthesis of AW compensators. However, such compensators typically fall into two categories: those which are simple in structure ([9], for example), but have few stability or performance guarantees; and those which are accompanied by these guarantees, but which suffer from a more complex structure ([17], for example). With few exceptions, the latter class of these techniques is normally only illustrated on simple, contrived examples [17]. In contrast, we present in this paper an application of an AW-design method, which has certain stability and performance properties, to an industrially relevant servo system.

The design approach used ensures that the AW compensator minimizes the effect of saturation on the system output. For this type of performance constraint, an $\mathcal{L}_2$-approach in combination with linear matrix inequality (LMI) optimization methods appears to be the most tractable for design. For AW control, this fact was first acknowledged in [18] for the design of a continuous-time AW compensator. In our case, we consider a discrete control problem and the $\mathcal{L}_2$-design ensures that during saturation, good closed-loop performance is achieved by being as close as possible to the nominal design, while the time interval for which the controller is saturated is minimized. Hence, the design procedure ensures that undue excitation of high-frequency resonances is kept close to the minimum possible when the control signal saturates at the limits recommended by the manufacturer. Thus, the paper demonstrates a novel discrete-time AW design method developed in [29] by applying it to the servo-control system of a hard disc drive with secondary actuator, which is novel in its own right.

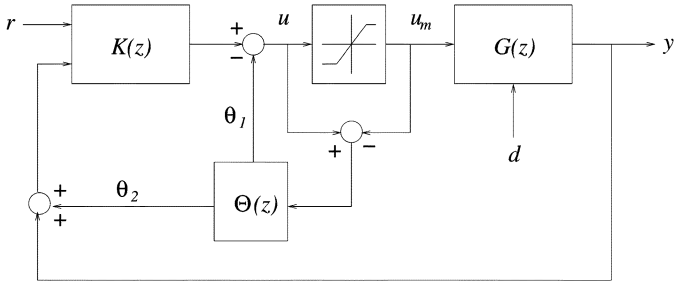

Fig. 2. General AW configuration.

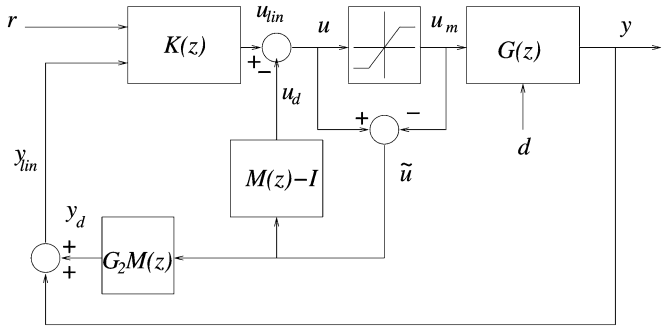

Fig. 3. Conditioning with $M(z)$.

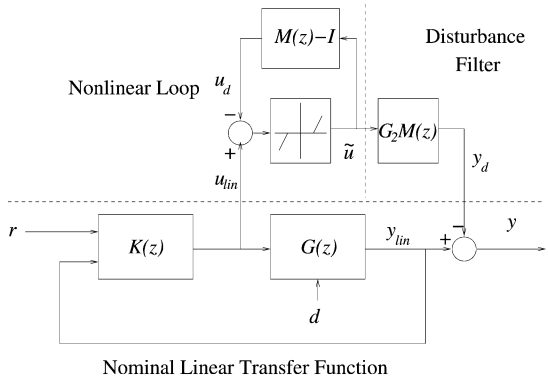

Fig. 4. Equivalent representation of conditioning with $M(z)$.

II. Anti-Windup Compensation

The type of AW compensation we consider is shown in Fig. 2, where $y = G[d' u_m']', G = [G_1\ G_2]$, represent the nominal plant with disturbances d; K is the controller; and $\Theta(z) = [\Theta_1(z)'\ \Theta_2(z)']'$ is the AW compensator, which becomes active if saturation occurs. Although this representation is fairly general, it is difficult to analyze the stability and performance properties of the system in Fig. 2. Instead of attempting a direct analysis of this configuration, it is convenient to think of AW in terms of $M(z)$, as depicted in Fig. 3, which was introduced in [32]. As demonstrated in [32], with all signals labeled identically, Fig. 3 can be redrawn as Fig. 4, which exhibits an attractive decoupling into a nominal linear system, disturbance filter, and nonlinear loop. The two equivalent AW control configurations from Figs. 3 and 4 imply a simple approach to AW design, the internal model control (IMC) scheme which is explained next.

A. IMC-Type AW-Approach

From Fig. 4, an AW-scheme follows, which is stable for all asymptotically *stable linear plants*; simply set $M(z) = I$ so that $\Theta_1(z) = 0$ and $\Theta_2(z) = G_2$ in Fig. 2. However, this AW configuration and the IMC solution, has the drawback that it requires a compensator of order equal to that of the plant to be used, which is not usually acceptable. Furthermore, the IMC solution is known, in many cases, to yield a poor transient performance (see [6] and [31] for some examples). Nevertheless, the IMC-scheme as a well established AW-scheme [6], [31] is known to provide a robustly stabilizing AW-solution [27]. This robustness characteristic will be verified experimentally. Hence, it appears to be reasonably intuitive to improve on the IMC-compensation method as one of our approaches to AW-compensation.

The first step is to reduce the order of the IMC-AW compensator. Hence, the natural strategy to follow is to see whether a reduced order version of $G_2(z)$ will work instead, i.e., use $\Theta_2(z) = \hat{G}_2(z)$ instead of $G_2(z)$, where $\hat{G}_2(z)$ denotes an order-reduced version of $G_2(z)$. Suitable tools for the stability analysis of this IMC-type AW-compensator with reduced order plant model $\hat{G}_2(z)$ and a subsequent approach toward improving the performance of the IMC-type compensator are presented next.

B. Low-Order Suboptimal Compensation

Based on the IMC-type AW-approach, choose the structure of $\Theta(z)$ from Fig. 2 as

$$\Theta(z) = \begin{bmatrix} \Theta_1(z) \\ \Theta_2(z) \end{bmatrix} = \begin{bmatrix} F_1(z)\tilde{\Theta}_1 \\ \hat{G}_2(z)\tilde{\Theta}_2 \end{bmatrix} \tag{1}$$

where $F_1(z), \hat{G}_2(z)$ are two Schur stable transfer function matrices, and $\tilde{\Theta}_1, \tilde{\Theta}_2$ are two static matrices, of appropriate dimensions. The matrix, $\tilde{\Theta} = [\tilde{\Theta}_1' \tilde{\Theta}_2']'$ is to be optimized for AW performance. For this, we may interpret this type of AW compensation in terms of that in Fig. 3. The expression for the control signal, u, is given, for the two schemes, by

$$u = K_1 r + K_2 y + (K_2\Theta_2 - \Theta_1)\tilde{u} \tag{2}$$

$$u = K_1 r + K_2 y - [(I - K_2 G_2)M - I]\tilde{u} \tag{3}$$

as computed from Figs. 2 and 3, respectively, using $K = [K_1 \; K_2]$. For these to be equivalent we must have

$$M = (I - K_2 G_2)^{-1}(-K_2\Theta_2 + \Theta_3) \tag{4}$$

where $\Theta_3 := \Theta_1 + I$.

From Fig. 4, it can be seen that the performance degradation and the system experiences during saturation is directly related to the mapping $\mathcal{T} : u_{\text{lin}} \mapsto y_d$ and, hence, the size of this mapping is an important measure of the performance of our AW compensator (see [28] for a discussion of this in continuous time, and [29] for the discrete-time counterpart). For performance optimization, we attempt to choose $\Theta(z) = [\Theta_1(z)' \; \Theta_2(z)']'$ such that a performance measure for the operator $\mathcal{T}$ is minimized. Due to the practical and theoretical tractability of l_2-constraints[1], it is attractive to minimize the l_2-gain, $\|\mathcal{T}\|_{i,2}$, of the operator $\mathcal{T}$

$$\|\mathcal{T}\|_{i,2} = \sup_{0 \neq u_{\text{lin}} \in l_2} \frac{\|y_d\|_2}{\|u_{\text{lin}}\|_2}$$

considering the l_2-norm $\|x\|_2$ of a discrete signal $x(k), (k = 0, 1, 2, \ldots)$

$$\|x\|_2 := \sqrt{\sum_{k=0}^{\infty} \|x(k)\|^2}.$$

Using this approach, an AW-compensator which minimizes in a suboptimal fashion the l_2-gain of the operator $\mathcal{T}$, can be computed. It was shown in [29], from a more general, nonstandard form of the *circle criterion*, that a compensator of the form given in (1) can be calculated by solving the LMI of (5) in the variables $L, Q > 0$, diagonal $U > 0$ and the positive real scalar $\gamma > 0$. The l_2-gain bound of $\mathcal{T}$ is given by γ and the compensator achieving this bound is given by (1) where $\tilde{\Theta} = [\tilde{\Theta}_1' \; \tilde{\Theta}_2']'$ is calculated as $\tilde{\Theta} = LU^{-1}$. The structure of the other constant matrices is given in the Appendix, but essentially follow by calculating the state-space matrices associated with $(M - I)$ and $G_2 M$ using (4) (as shown in (5) at the bottom of the page).

From (1), it can be easily seen that the IMC-type solution is recovered for $[\tilde{\Theta}_1' \; \tilde{\Theta}_2']' = [0 \; I]'$ irrespective the choice of $F_1(z)$. Thus, the stability of the IMC-type approach is established once the LMI of (5) is satisfied for large enough $\gamma > 0$. Generally, the existence of solutions to the LMI of (5) and respectively the existence of an l_2-gain for the operator $\mathcal{T}$ guarantees *global* (exponential) stability of the closed-loop system in the face of actuator saturation.

1) Choosing the Dynamics of $\Theta_1(z)$: For the selection of $\Theta_1(z)$, it is desirable to limit the high-frequency activity of $\Theta_1(z)$, as this affects the control signal directly. Hence, $F_1(z)$ may be chosen as a bank of first-order low-pass filters, for which $\deg(F_1(z)) = m$, where m is the dimension of the control vector. The total order of the compensator is thus given by

$$\deg(\Theta(z)) = \deg(F_1(z)) + \deg(\hat{G}_2(z)). \tag{6}$$

[1]We use the notation l_2 to represent the discrete-time counterpart of $\mathcal{L}_2$

$$\begin{bmatrix} -Q & -Q\bar{C}_1' & Q\bar{A}' & 0 & Q\bar{C}_2' \\ \star & -2U - D_{01}U - \bar{D}_1 L - UD_{01}' - L'\bar{D}_1' & UB_0 + L'\bar{B}' & I & UD_{02}' + L'\bar{D}_2' \\ \star & \star & -Q & 0 & 0 \\ \star & \star & \star & -\gamma I & 0 \\ \star & \star & \star & \star & -\gamma I \end{bmatrix} < 0 \tag{5}$$

TABLE I
PROCEDURE FOR ANTI-WINDUP CONTROLLER DESIGN AND IMPLEMENTATION

	IMC-type-AW	*suboptimal AW*	*full-order AW*
Step 1	Plant Modelling: $G_2 \sim (A_p, B_p, C_p, D_p)$		
Step 2	Nominal Linear Controller Design: $K(z)$ (see Figures 2 and 3)		
Step 3	Choose a reduced order representation $\hat{G}_2 \sim (A_2, B_2, C_2, D_2)$ of the plant		*Not Applicable*
Step 4	Choose $F_1 = 0$.	Choose a bank of low pass filters $F_1 = diag(F_{11}, ..., F_{1m})$	*Not Applicable*
Step 5	Compute the augmented plant variables $\bar{A}$, $\bar{B}$, B_0, $\bar{C}_1$, $\bar{C}_2$, D_{01}, D_{02}, $\bar{D}_1$, $\bar{D}_2$ using the Appendix		*Not Applicable*
Step 6	Compute an initial solution for the LMI of (5) using (7) and $U = I$ and $\tilde{\Theta} = [0\ I_m]'$		*Not Applicable*
Step 7	Verify stability by *testing* if there is $\gamma > 0$ satisfying LMI (5)	Solve LMI of (5) by *minimizing* γ and compute $\tilde{\Theta} = LU^{-1}$	Solve the LMI of (9) using (A_p, B_p, C_p, D_p) by minmizing μ and compute $F = LQ^{-1}$
Final Step	according to Figure 2 and $\Theta = [0\ \ \hat{G}_2^T]^T$	*Implement* the AW-compensator according to Figure 2 using equ. (1)	according to Figure 3 using equ. (8) and $G_2(z)M(z) = N(z)$

2) Initialization of the Low-Order AW-Compensator LMI-Routine: For l_2-optimization in the low-order AW case, the l_2-gain, γ, is to be minimized using the linear matrix inequality of (5) in the variables $Q \in \mathbb{R}^{m_Q \times m_Q}, U \in \mathbb{R}^{m \times m}$ and $L \in \mathbb{R}^{2m \times m}$. This requires that the LMI-optimization routine finds a proper initial value for the large size matrix Q, where

$$m_Q = \deg(F_1(z)) + \deg(\hat{G}_2(z)) + \deg(G_2) + \deg(K_2)$$

as can be verified from the LMI of (5) and the Appendix. For such a large optimization problem, we found that the LMI-solvers of the Matlab-LMI-Toolbox[2] do not necessarily provide an initial feasible solution, despite the existence being theoretically shown. However, employing the Matlab-command *dare*, the following discrete algebraic Riccati equation in X can be used for initialization

$$\bar{A}'X\bar{A} - (\bar{A}'X\tilde{B} + S)(\tilde{B}'X\tilde{B} + R)^{-1} \times (A'X\tilde{B} + S)' + \delta_1 I = 0 \quad (7)$$

where $R = -2U^{-1} - U^{-1}(D_{01} - \bar{D}_1\tilde{\Theta}) - (D_{01} + \bar{D}_1\tilde{\Theta})'U^{-1} + \delta_2 I, S = (-\bar{C}_1'U^{-1})$, and $\delta_1, \delta_2 > 0$, and $\tilde{B} = (B_0 + \bar{B}\tilde{\Theta})$. If there exists a solution X to (7), for a reasonable guess of $\delta_1, \delta_2, \tilde{\Theta}$, and U, then it can be shown using the Schur complement and an equivalent congruence transformation that the LMI of (5) is satisfied for large enough value $\gamma > 0$ and $Q = X^{-1}$. Suitable choices for U and $\tilde{\Theta}$ should coincide with the IMC-case, i.e., $U = I$ and $\tilde{\Theta} = [0\ I_m]'$ where I_m is the $m \times m$-identity matrix. For a solution of the Riccati equation of (7), in particular, the leading principal minor of size $(2m_Q + m) \times (2m_Q + m)$ of the LMIs left-hand matrix in (5) is negative definite.

C. Full-Order AW-Compensation

If higher order controllers are acceptable and performance is of primary concern, it is suitable to allow the order of the AW-compensator to be full-order, hence, the same order as the plant model. In this case, $M(z)$ can be chosen as a coprime factor of $G_2(z)$ in the same way as in [32] for the continuous-time AW case. So if $G_2(z) = N(z)M^{-1}(z)$, we can search for a coprime factorization of $G(z)$ such that the AW closed-loop has the best performance in terms of $\|\mathcal{T}\|_{i,2}$. To achieve full-order stabilization, we would like to choose coprime factors, which share the same state space and have order equal to that of $G_2(z)$. Employing Fig. 4, such coprime factorizations can be characterized by

$$\begin{bmatrix} M(z)-I \\ N(z) \end{bmatrix} \sim \begin{bmatrix} x_p(k+1) \\ u_d(k) \\ y_d(k) \end{bmatrix} = \left[\begin{array}{c|c} A_p + B_pF & B_p \\ \hline F & 0 \\ C_p + D_pF & D_p \end{array}\right] \begin{bmatrix} x_p(k) \\ \tilde{u}(k) \end{bmatrix} \quad (8)$$

for $G_2 \sim (A_p, B_p, C_p, D_p), A_p \in \mathbb{R}^{n \times n}, B_p \in \mathbb{R}^{n \times m}, C_p \in \mathbb{R}^{p \times n}, D_p \in \mathbb{R}^{p \times m}$ and a discrete-time state vector $x_p \in \mathbb{R}^n$ [34]. Note that (8) is parameterized by the free parameter F which is to be optimized. It was proved in [29], that a compensator of the form given in (8), which minimizes the l_2-gain, $\|\mathcal{T}\|_{i,2}$, can be calculated by solving the LMI

$$\begin{bmatrix} -Q & -L' & 0 & QC_p' + L'D_p' & QA_p + L'B_p' \\ \star & -2U & I & UD_p' & UB_p' \\ \star & \star & -\mu I & 0 & 0 \\ \star & \star & \star & -I & 0 \\ \star & \star & \star & \star & -Q \end{bmatrix} < 0 \quad (9)$$

for $Q > 0, U = \mathrm{diag}(\mu_1, \ldots \mu_m) > 0, L \in \mathbb{R}^{m \times n}$. Furthermore, if this inequality is satisfied, a suitable F for (8) achieving $\|\mathcal{T}\|_{i,2} < \gamma = \sqrt{\mu}$, is given by $F = LQ^{-1}$. Note that it has been shown in [29] that there is always a solution to the full-order AW problem. As for the low-order AW-compensator, the existence of a solution to the LMI (9) ensures global (exponential) stability of the AW scheme.

D. AW-Design Procedure

In summary, the design and implementation of the three AW methods, the IMC-based, the sub-optimal low order and the optimized full-order AW compensator, follow the eight steps as given in Table I. Note that the steps 5–7 listed for the IMC-type

[2]The Mathworks Inc.

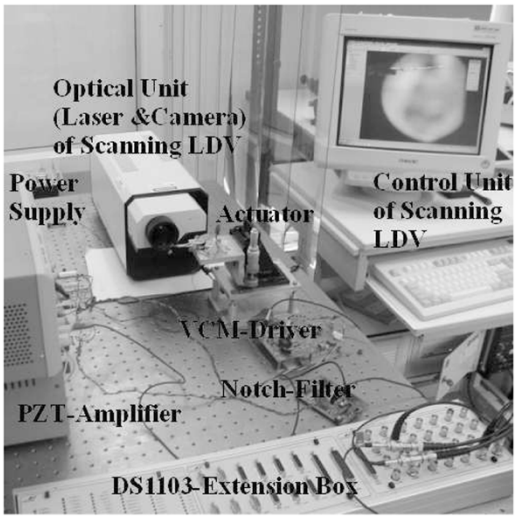

Fig. 5. Experimental setup.

AW-compensator are introduced to verify nominal stability of the scheme.

III. Actuators and Actuator Modelling—Step 1

This section presents the measured actuators and actuator models subsequently used for controller design. For measurement of the tip position of the PZT-secondary actuator [25] (Fig. 5), we used a Laser-Doppler-Scanning-Vibrometer[3] (LDV).

A. The Actuators

For each actuator, 12 frequency responses were measured via a Dynamic Signal Analyzer[4] (DSA) as presented in Figs. 6 and 7. The PZT-actuator features significant resonances at frequencies of 9.97, 20, and 34 kHz (Fig. 7). The smaller resonances at 7.2 and 12 kHz are not that important for controller design and the actual practical results. However, the two pronounced high-frequency resonances at 20 and 34 kHz can create significant aliasing effects because controller sampling frequencies below 30 kHz are usually used. Thus, a hardware anti-aliasing filter combined with a notch-filter has been employed to attenuate in particular the PZT-actuator resonance at 20 kHz (Fig. 7). Note, from Fig. 7, that the anti-aliasing filter has a maximum absolute gain of 0.5 and it shifts the low-frequency phase response by 180° since an inverting operational amplifier circuit has been incorporated for input–output impedance adjustment.

B. The Actuator Models—Continuous and Discrete

From the frequency response measurements, we derived the continuous linear nominal PZT- and VCM-actuator models via curve fitting. These models have high orders of 18 and 13, respectively, to represent high-frequency resonances, which are vital to obtain a high bandwidth controller.

Noting that the micro-actuator has significant resonances at 20 and 34 kHz, while a servo-bandwidth of more than 2 kHz is targeted, an intuitive solution is to use a multirate control

[3]Polytec OFV 3001S, Polytec, Waldbronn, Germany.

[4]HP 35 670A, Hewlett Packard Company, Washington.

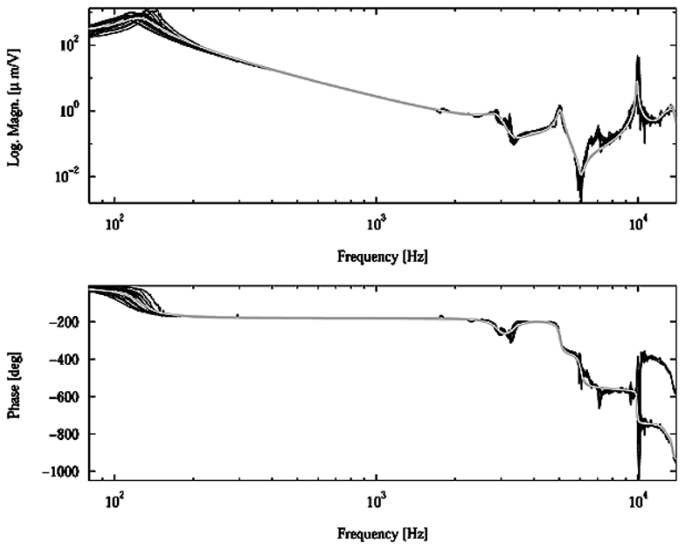

Fig. 6. VCM-frequency responses (including VCM-voltage-to-current driver). Measured: dark. Nominal transfer function: light.

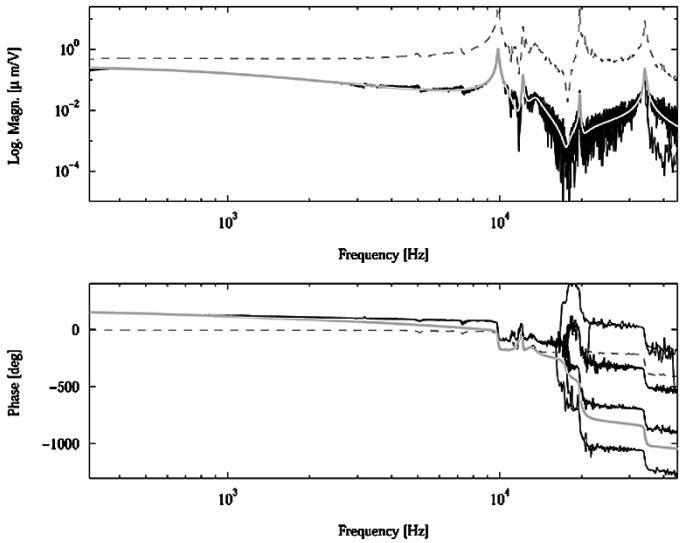

Fig. 7. PZT-frequency responses (including PZT amplifier and notch filter); measured (with notch filter). Dark: nominal transfer function (with notch filter). Light: measured without notch filter: dashed.

scheme [11], [23] to compensate for the resonances. In our case, we found that considerable suppression of aliasing effects and significant order reduction for the model employed in the controller design is possible when a single sampling frequency of 22 kHz is used. It is easily verified that the zeroth-order hold aliasing image of the PZT-actuator resonance at 34 kHz can be found at 10 kHz. Hence, the two PZT-actuator resonances at 9.97 and 34 kHz appear at the same frequency for the zeroth-order hold discrete-time model. As a result, a seventh-order discrete PZT-actuator model and an eleventh-order discrete VCM-model have been used for the nominal plant model $G_2 = [G_{\rm VCM}\ G_{\rm PZT}]$ in the subsequent compensator design.

We will see in Section VI that this choice for the sampling time ensured the successful suppression of high-frequency resonances of the actuator. Nevertheless, in practice, actuator to actuator resonance variations of $\pm 5\%$ are possible. For this,

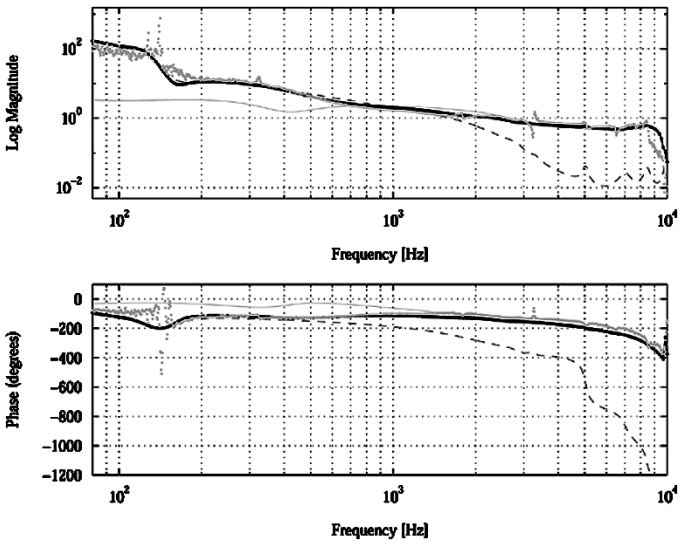

Fig. 8. Open-loop responses, PZT-loop ($K_{\rm PZT}G_{\rm PZT}$): light thin line, VCM-loop ($K_{\rm VCM}G_{\rm VCM}$): thin dashed, combined nominal ($K_{\rm VCM}G_{\rm VCM}+K_{\rm PZT}G_{\rm PZT}$): thick black dot-dash, measured loop: thick dot.

numerical tests confirmed that a change of the PZT-actuator high frequency resonance at 34 kHz by $\pm 10\%$ to 37.5 and 31 kHz retain the aliasing image sufficiently close to the Nyquist frequency of 11 kHz. Assuming a good controller roll-off, phase and gain margins are affected by less than 1% as can be easily verified for the controller design presented in the next section. This also has the effect that the stability of the simulated AW-schemes remains unaffected.

IV. Linear Controller Design—Step 2

Employing the nominal plant model $G_2=[G_{\rm VCM}\ G_{\rm PZT}]$, we chose for control the standard one-degree of freedom structure, $K_1=[K_{\rm VCM}\ K_{\rm PZT}]', K_2=-K_1$, as it easily allows robust linear design techniques to be employed. For design, the worst-case magnitude [10] for the relative uncertainty of both actuators was evaluated using the frequency measurements and the nominal frequency response (Fig. 6). These frequency-dependent uncertainty models along with a high-bandwidth performance target in terms of a desired frequency response for the closed-loop system can be used as weights in a robust, discrete μ-control analysis and synthesis [10]. A single-input dual-output controller $[K_{\rm VCM}\ K_{\rm PZT}]'$ of twelfth order for each element, $K_{\rm VCM}$ and $K_{\rm PZT}$, achieving a nominal open-loop bandwidth of 2.4 kHz, a gain margin of 4.6 dB, and a phase margin of 36.3°, was designed using this discrete μ-synthesis approach. This matches well the experimentally measured frequency response (Fig. 8). Note from Fig. 8, that the PZT-loop is activated only at high frequency as the controller hand off [22] is larger than 700 Hz. Based on these linear controllers, the AW compensators are designed next.

V. The AW-Compensator Design—Steps 3–7

All of the three discussed AW controller design strategies, the IMC-type approach ($\Theta_1=0, \Theta_2=\hat{G}_2$), the low-order AW-approach and the full-order AW controller have been tested.

A. IMC-Type AW-Compensator

As mentioned in Section II-A, the choice for Θ_2 for the AW-configuration of Fig. 2 is a reduced order plant $\hat{G}_2$ which was in this case order 14, while $\Theta_1=0$. Hence, in terms of the AW-scheme of (1), this is equivalent to $F_1(z)=0$, and $[\tilde{\Theta}_1'\ \tilde{\Theta}_2']'=[0\ I]'$; and the selection assures that the LMI of (5) can be initialized via the Riccati equation (7) assuring theoretically stability of the compensator. Experimental tests showed that the controller remains also practically stable suppressing reasonably well high-frequency vibrations.

B. Filter Choice and LMI-Optimization for Low-Order AW

For design of the suboptimal AW controller, it is important to consider that the PZT-control signal always saturates before the VCM-actuator signal reaches its saturation limit. Hence, the primary concern for the AW compensator design is the "small" signal behavior of the AW compensator, i.e., the characteristics for saturated PZT-control signal only.

1) *Choice of* $\hat{G}_2$ As in 14-th order reduced plant model $\hat{G}_2(z)$ is used.
2) *Choice of* F_1 As the output of the filter $F_1=\mathrm{diag}(F_{11},F_{21})$ feeds directly into the control signal, it appeared reasonable to choose F_1 to have some low-pass characteristic to preserve robustness and to suppress the excitation of high-frequency plant resonances. In our experiments, it appeared to be advisable for F_1 to emulate a continuous-time low-pass filter with a pole of magnitude not larger than $2\pi 3000$.

For F_{21}, the filter mainly affecting the PZT-actuator, we tested a filter closely matching a continuous-time low-pass filter with a fast pole of magnitude at $2\pi 3000$ and another relatively slow pole of magnitude at $2\pi 800$. As demonstrated later, the filter F_{21} with the fast pole appeared to be beneficial when considering control action for saturated PZT-control signal caused by step responses of large magnitude. In contrast, the filter with slow pole seemed to benefit the performance for a step response of *small* magnitude and saturated PZT-control signal, although this benefit came with the tradeoff of decreased robustness. These observations will be discussed in more detail when presenting the experimental results in Section VI.

For F_{11}, we also chose a discrete filter emulating a continuous-time pole at $2\pi 3000$ as it generates acceptable results.

Accordingly, the two investigated different configurations for F_1 are

$$\begin{aligned}\mathrm{Config.1}: F_{11}&=\frac{0.58}{z-0.42}\\ F_{21}&=\frac{0.20}{z-0.80}\approx \text{cont. pole at } 2\pi 800 \quad (10)\\ \mathrm{Config.2}: F_{11}&=\frac{0.58}{z-0.42}\\ F_{21}&=\frac{0.58}{z-0.42}\approx \text{cont. pole at } 2\pi 3000 \quad (11)\end{aligned}$$

1) l_2-Characteristics and LMI-Initialization: For the suboptimal AW controller design, we had to limit the structure of $\tilde{\Theta}_2$ from (1) to a diagonal matrix $\tilde{\Theta}_2=\mathrm{diag}(\tilde{\Theta}_{12},\tilde{\Theta}_{22})$, constraining the optimization process to use the structured matrix $\tilde{\Theta}=[\tilde{\Theta}_1'\ \tilde{\Theta}_2']'$. A nondiagonal $\tilde{\Theta}_2$ can cause AW compensator

action in the VCM-controller channel for saturated PZT-control signal. Practically, this was not found viable in the suboptimal case, as the nondiagonal, optimized matrix $\tilde{\Theta}_2$ would cause a very slowly oscillating step response with unacceptably long settling time once the PZT-control signal is saturated. Hence, by removing the AW controller action in the VCM-controller channel for saturated PZT-control signal, this characteristic was suppressed.

To motivate the structural constraint for $\tilde{\Theta}_2$, it must be noted that the LMIs of (5) and (9) have been derived to achieve nominal global stability and to optimize the l_2-gain $\|\mathcal{T}\|_{i,2}$ in a *global sense* irrespective of the signal amplitudes. For linear systems, the l_2-gain is not dependent on the amplitude, but as the AW compensator contains the saturation nonlinearity, local, and global l_2-gain analysis will typically yield different results, meaning that the small and large signal behavior can be significantly different. Although, the feature of global optimization seems to imply some disadvantage for either the designed small signal or the large signal characteristics of the AW compensator, it will be seen that the LMI-optimization can improve the IMC-type AW controller, while a structural constraint for $\tilde{\Theta}_2$ seems to resolve the problem for the small signal behavior of the suboptimal AW compensator. More investigations are required to understand this issue.

Along these guidelines, we restricted the structure of the variables of the LMI-routine for (5), while for initialization, we utilized (7) where $\delta_1 \approx 2\cdot 10^{-9}, \delta_2 \approx 10^{-2}$ and the initial value of γ was 600 000. Furthermore, we chose $U = I$ and $\tilde{\Theta} = [0\ I_2]'$ as initial values for (7) and (5).

2) LMI-Optimization: Configuration 1 with a low-pass filter combination from (10) has a gain matrix $\tilde{\Theta}$

$$\tilde{\Theta} = \begin{bmatrix} -0.6455 & 0.0014 \\ 4.0742 & -0.0811 \\ 0.3702 & 0 \\ 0 & 1.0049 \end{bmatrix} \tag{12}$$

for an l_2-gain $\gamma = 334.68$. Configuration 2 with the low-pass filters from (11) has a gain matrix

$$\tilde{\Theta} = \begin{bmatrix} -0.6693 & 0.0014 \\ 5.0282 & -0.1257 \\ 0.3503 & 0 \\ 0 & 0.9258 \end{bmatrix} \tag{13}$$

for $\gamma = 334.87$. Note that this l_2-gain is marginally higher than the l_2-gain for the IMC-type controller $(\gamma = 334.81)$ which is caused by an early termination of the LMI-algorithm due to a strict optimization termination constraint and a very high-initial value of γ =600 000.

C. Full-Order AW-Design

The full-order AW controller is designed using the LMI (9). Since the size of the full-order LMI-problem is not as great as for the suboptimal compensator, the LMI-optimization routines of the Matlab-LMI-Toolbox are sufficient to provide an initial solution for the full-order case. Thus, the minimal l_2-gain bound of $\mathcal{T}$ with the full-order AW compensator is 334.67.

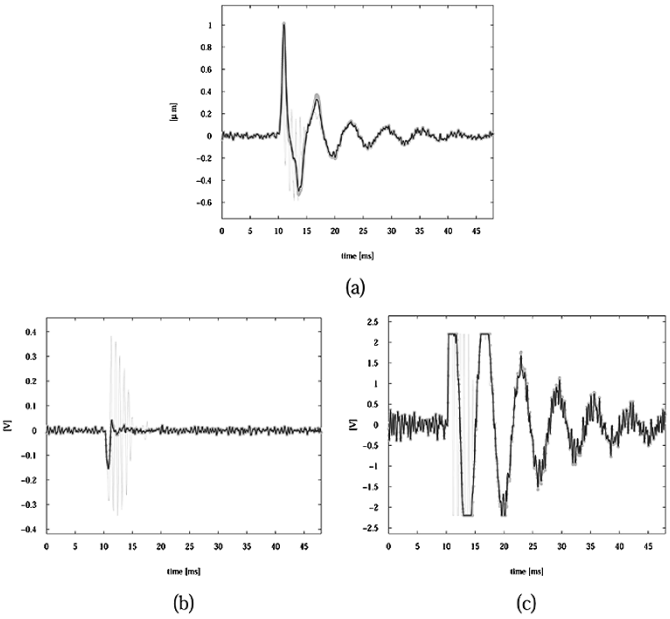

Fig. 9. Simulation results for shock disturbance evaluation; constrained linear control— thin light line, full order, and IMC-AW-compensator-thick line with thick dots; suboptimal AW-compensators-dark line. (a) Position signal. (b) VCM-control signal. (c) PZT-control signal.

VI. Implementation Results—Final Step 8

For practical controller implementation, the DSP based system, DS1103[5], was used with a sampling frequency of 22 kHz. The VCM-driver input voltage was kept in the interval $[-2V, 2V]$ employing the DS1103. The hardware anti-aliasing filter for the PZT-actuator was set in series with the PZT-amplifier to provide frequency filtering to the signal from the DS1103 before entering the PZT-amplifier. The DS1103 was used to limit the input signal to the anti-aliasing filter to the voltage range of $[-2.2V, 2.2V]$, which ensures that the input voltage into the PZT-elements of the actuator remain bounded as required. Hence, the *low frequency* displacement range is about ± 0.3 μm.

The AW configurations were investigated with respect to the following:

1) simulation tests for evaluation of the disturbance rejection;
2) practical step response tests for saturating PZT-actuator signal only;
3) practical step response tests for saturating PZT- and VCM-actuator signals.

A. Simulation Tests for Response to Shock Disturbances

Practically, it is difficult to evaluate the controller performance in response to shock disturbances because our setup has to remain stationary. Hence, simulation tests where carried out to evaluate the controller behavior with respect to a disturbance model from [3]. This simulation facility contains models for measurement noise, runout disturbances and torque disturbances. In addition, a half-sine shock disturbance of 1 ms

[5]DSpace DS1103 is a product of dSPACE GmbH, Paderborn, Germany.

[6]physical units of the signal of one oscilloscope channel see upper left of each image.

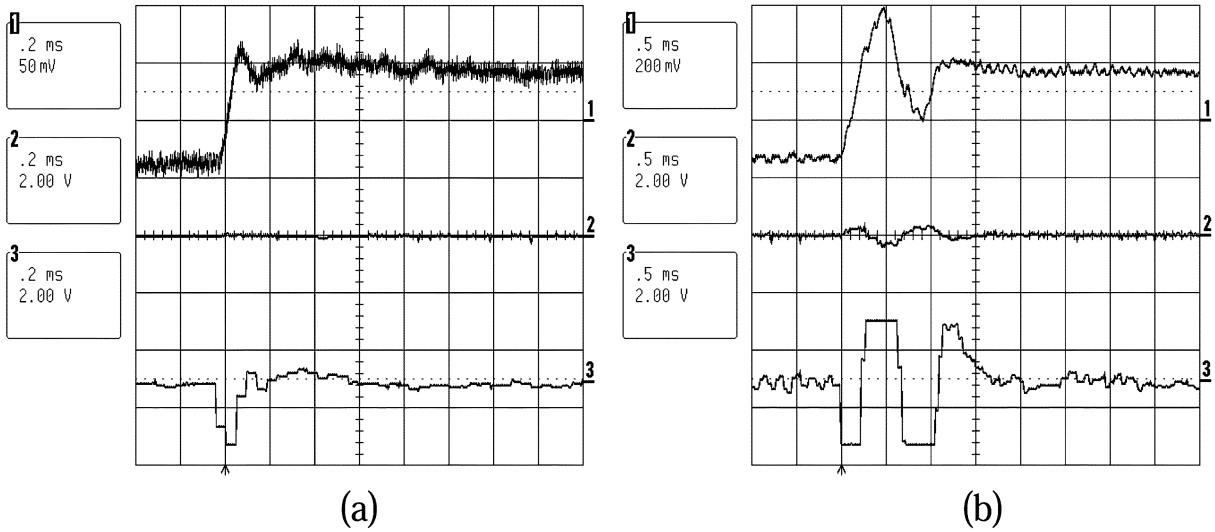

Fig. 10. Control without AW compensator. Ch 1: LDV-measurement (2 μm/V). Ch 2: VCM-driver input. Ch 3: PZT-control signal[6]. (a) 160 nm step, no saturation and (b) 600 nm step.

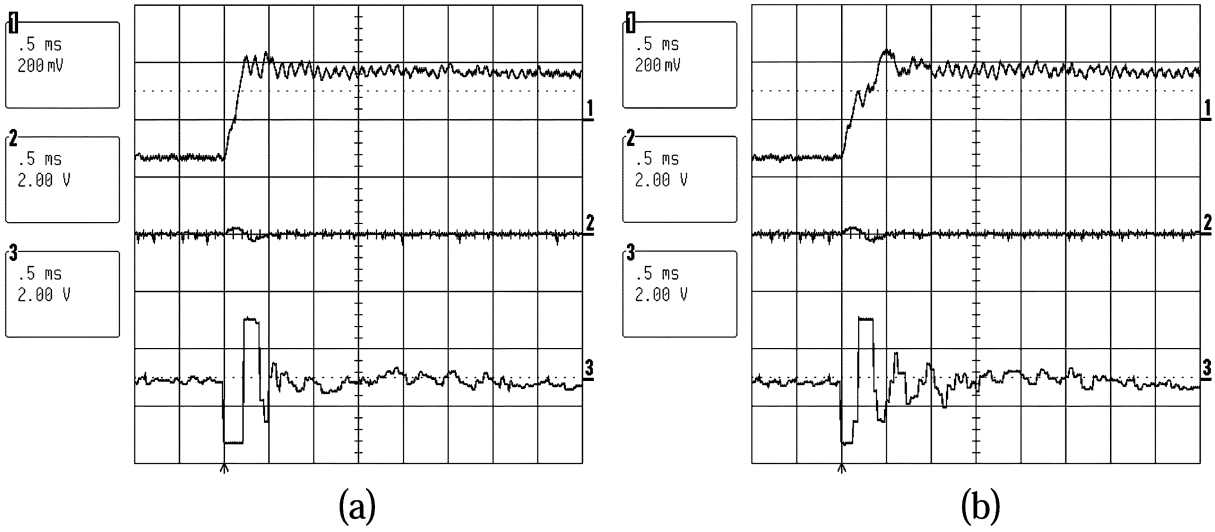

Fig. 11. A 600-nm step for control with AW compensator. Ch 1: LDV-measurement (2 μm/V). Ch 2: VCM-driver input. Ch 3: PZT-control signal. (a) Full order case. (b) IMC-type case.

duration was introduced at the input to the VCM-actuator at the time instant of 10 ms. The applied shock torque amplitude is about 7% of the torque available from the VCM-driver circuit. The linear controller without AW compensator but with control-signal limitations is marginally stable for this shock disturbance while all of the simulated AW-compensators remain stable for any shock disturbance amplitude. From Fig. 9, it is clear that the marginally stable control-limited linear controller, in comparison to the linear controller equipped with AW compensator, is subjected to significantly higher control activity in both the PZT-actuator and the VCM-actuator channel: High-frequency switching between saturation limits of the PZT-control signal can be observed for this case. In contrast, the control activity of the linear controller combined with AW-compensation is, for all AW-compensators, very similar, leading to the safe settling back onto the demanded track position with significantly less high frequency control action and PZT-control signal saturation.

B. Saturation of the PZT-Control Signal Only

Since it was difficult to recreate practically the conditions of shock disturbances, small controller step demands are tested to understand the response of the controller to a small shock-disturbance during track following.

The PZT-control loop has been designed to act in high frequency only (see open loop response on Fig. 8), so that it will be active only during the settling period, ensuring fast rise and settling times. Accordingly, it is expected that the PZT-control signal responds aggressively to a step demand and saturates at a step demand slightly below the allowable maximal displacement range. This has been verified via experimental tests showing that the input signal to the PZT-anti-aliasing filter saturates for a step demand of about 180 nm (see Fig. 10(a) for a 160-nm step demand response).

Once there is PZT-control signal saturation, the linear controller subjected to a step demand of 600 nm has a response

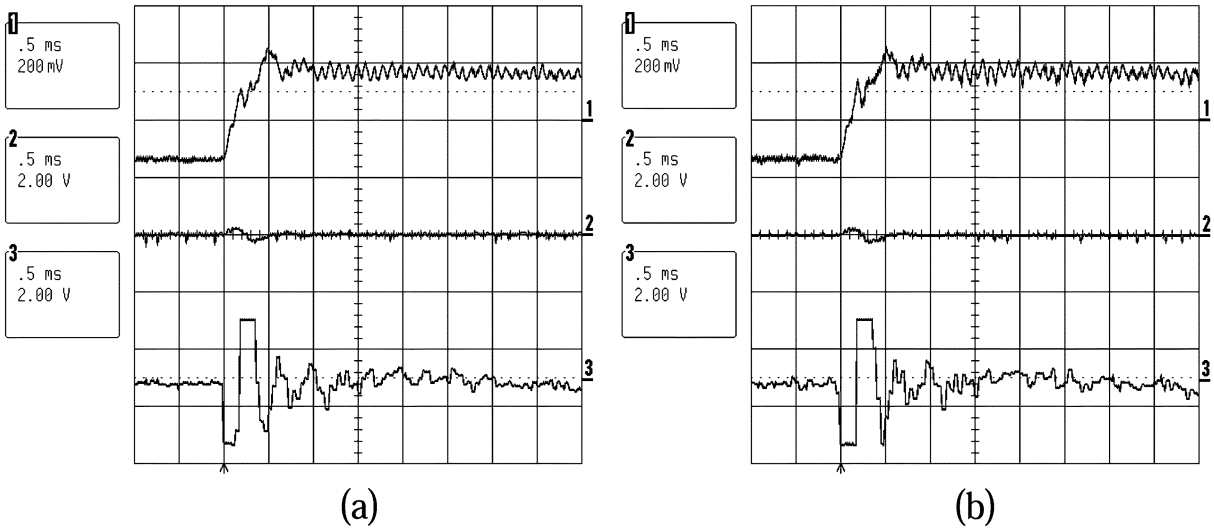

Fig. 12. A 600-nm step for control with AW compensator. ch 1: LDV-measurement. (2 μm/V). Ch 2: VCM-driver input. Ch 3: PZT-control signal. (a) Suboptimal case 1, (10), (12). (b) Suboptimal case 2, (11), (13).

TABLE II
MAXIMAL ALLOWABLE STEP DEMAND AMPLITUDE FOR CLOSED-LOOP STABILITY

	without AW	IMC-AW	subopt. conf. 1	subopt. conf. 2	full-order AW
amplitude [μ m]	0.618	1.8	1.9	5.6	4

with a large overshoot of more than 60% and the settling time increases from less than 0.3 to 1.5 ms due to PZT-control signal saturation [Fig. 10(b)]. The introduction of an AW compensator for this step demand improves this slow settling behavior significantly. All of the AW-compensators suppress the overshoot and improve the settling behavior to values of less than 1 ms (Figs. 11 and 12). The full-order AW controller shows superior performance with respect to suppression of high-frequency oscillations, and it has about 25% faster rise time than the IMC-type controller and the suboptimal AW-scheme. The results for the two re-optimized and sub-optimal AW compensators show characteristics very similar to the IMC-type AW case. However, the sub-optimal AW configuration 2 from (11) and (13) introduces some undesirable high-frequency oscillation [Fig. 12(b)]. Nevertheless, this characteristic must be balanced against its superior performance for a higher controller demand amplitude.

In the case of a of 1.6-μm step demand, the linear controller without AW compensation was unstable (Table II). Although, the full-order AW compensator has, in comparison to the other three AW compensators of Fig. 13, the largest step response overshoot, the PZT-control signal recovers decisively faster from the saturation with a settling time of 0.7 ms, while the settling for all other AW compensators is extended to at least 1.9 ms. Note that both suboptimal AW controllers resume faster nominal linear control action than the IMC-type compensator, which results in shorter settling times. In this case, the suboptimal compensator configuration 2 with low-pass filters of large bandwidth performs better than the sub-optimal compensator configuration 1 from (10) and (12).

C. Saturation of Both Control Signals

The case of large step demands is mainly of *academic* interest, as it demonstrates the compensator robustness, and it shows some interesting features of the AW compensators. This case should only occur for large track seek demands for which a *dedicated seeking control* method *might be preferred.*

When both actuator signals saturate, the IMC-type controller and the suboptimal controller configuration 1 of (10) and (12) are unstable. For a step demand of 3.6 μm, the full-order AW compensator and also the suboptimal AW configuration 2 from (11) and (13) show an overshoot of more than 50%. However, the suboptimal AW compensator takes a significantly longer time to recover from the VCM-control signal saturation and also from the PZT-control signal saturation. As a result, the settling time of the response for the suboptimal compensator of about 11 ms is nearly five times larger than for the full-order AW controller.

For a larger demand amplitude of 5.2 μm, the suboptimal AW configuration 2 remains stable, while all other AW compensators are outside their stability range as documented in Table II. The suboptimal AW configuration 2 yields step responses of long settling times and an overshoot of more than 100% as documented in Fig. 15.

VII. DISCUSSION

Although, all three AW-compensators were designed to be globally stable, each remained stable during the practical test for a certain range of step demand amplitudes only. Nevertheless, the AW-compensators significantly improved the stability region when compared to the uncompensated linear controller as documented in Table II. The compensator with the largest stability region was the suboptimal compensator configuration 2 from (11) and (13) which remained stable for a saturated VCM-actuator signal. The full-order AW compensator had a similar but slightly smaller stability region, again providing stable step responses for a saturating VCM-actuator signal. The IMC-type AW compensator yielded a smaller stability region, with the

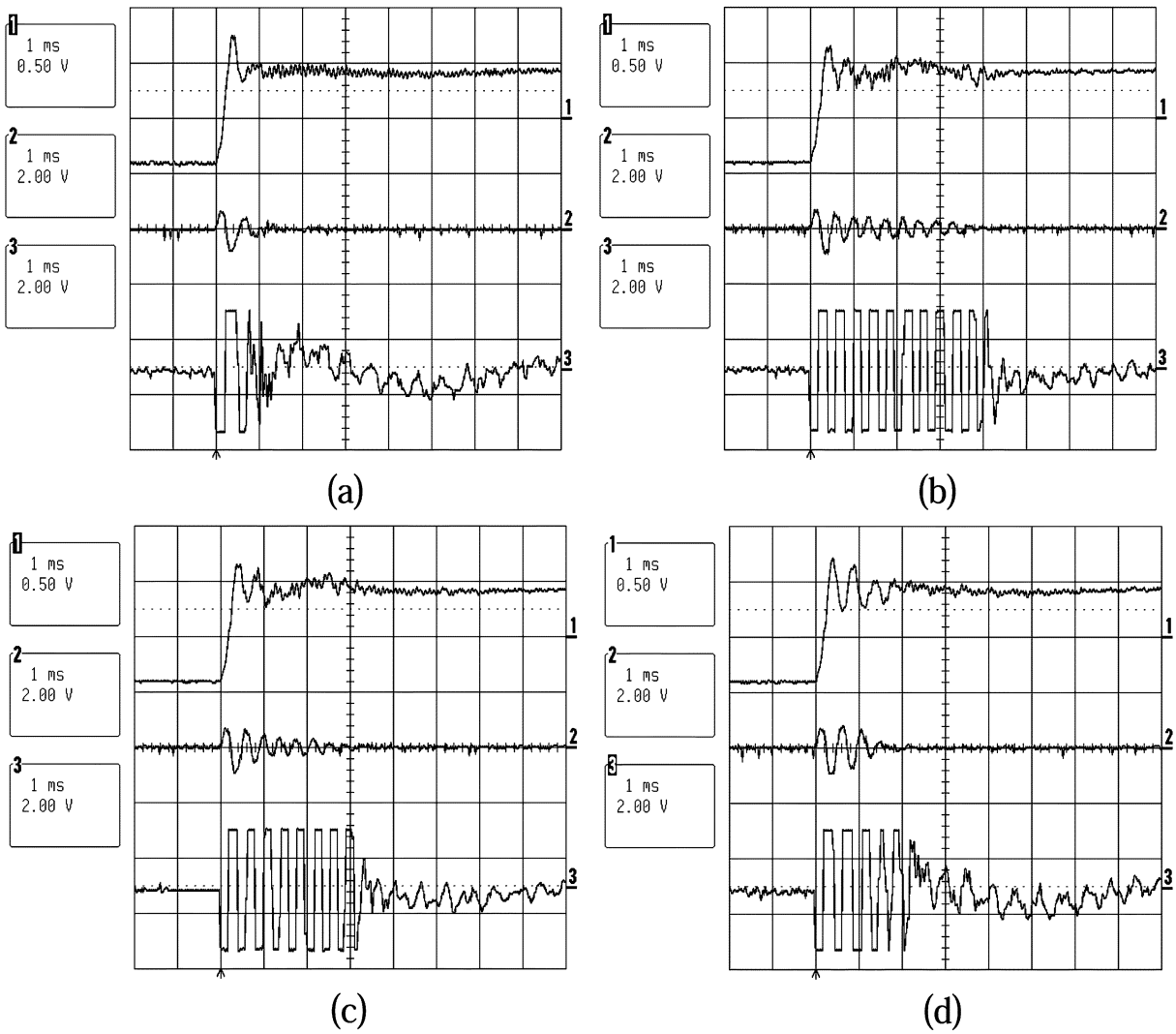

Fig. 13. 1.6 μm step for control with AW compensator. Ch 1: LDV-measurement (2 μm/V). Ch 2: VCM-driver input. Ch 3: PZT-control signal. (a) Full-order case. (b) IMC-type case. (c) Suboptimal case 1, (10), (12). (d) Suboptimal case 2, (11), (13).

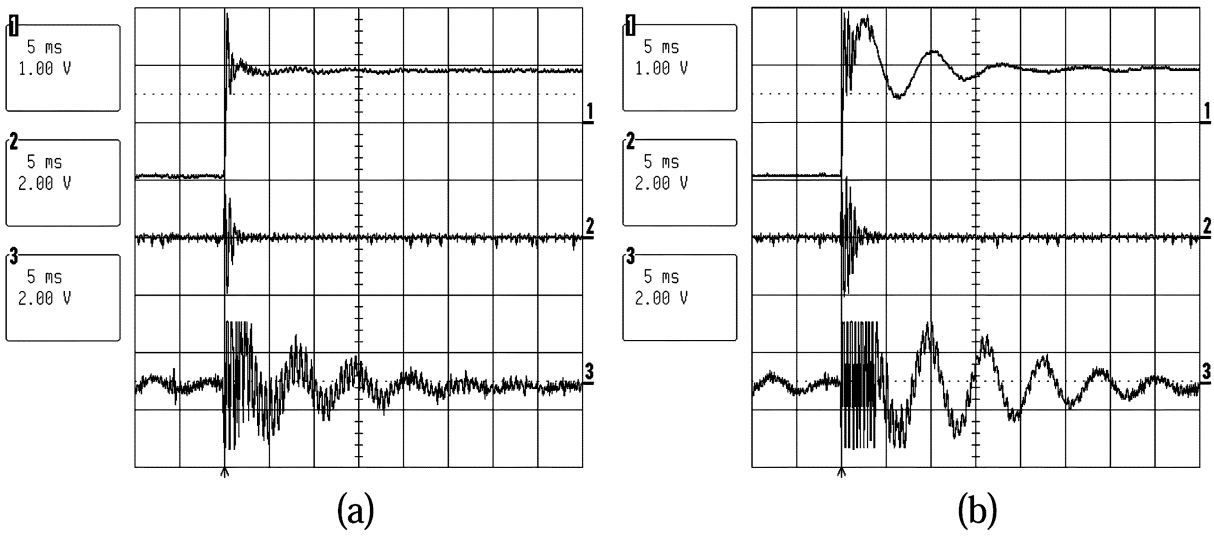

Fig. 14. 3.6 μm step for control with AW compensator. Ch 1: LDV-measurement (2 μm/V). Ch 2: VCM-driver input. Ch 3: PZT-control signal. (a) Full-order case. (b) Suboptimal case 1 (11) and (13).

TABLE III
DYNAMIC CHARACTERISTICS: t_s-SETTLING TIME, $t_{\rm rec}$-TIME FOR CONTROLLER TO RECOVER FROM SATURATION

amplitude [μ m]	without AW [m s]		IMC-AW [m s]		suboptimal AW config. 1 [m s]		suboptimal AW config. 2 [m s]		full-order AW [m s]	
	t_s	t_{rec}	t_s	t_{rec}	t_s	t_{rec}	t_s	t_{rec}	t_s	t_{rec}
0.16	0.3	0	0.3	0	0.3	0	0.3	0	0.3	0
0.6	1.5	1	1	0.3	0.8	0.3	1	0.5	0.6	0.4
1.6	NA	NA	3.8	4.1	3	3.2	1.9	2.2	0.7	0.8
3.6	NA	NA	NA	NA	NA	NA	11	10.3	2.4	2.4
5.2	NA	NA	NA	NA	NA	NA	25.3	29.2	NA	NA

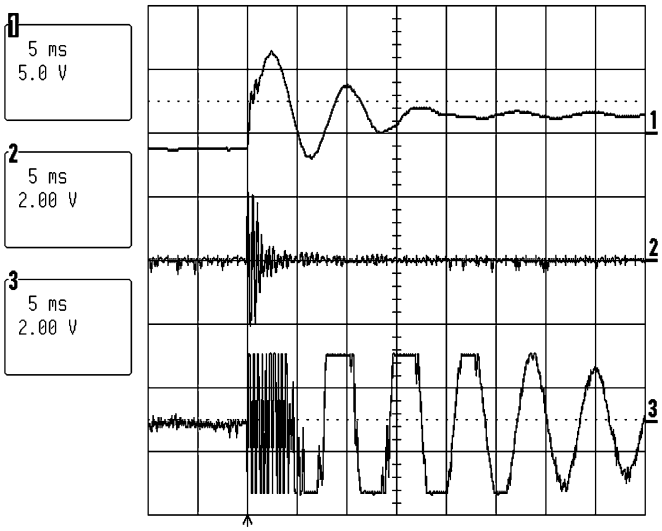

Fig. 15. 5.2 μm step for control with suboptimal AW compensator 2 of (11) and (13). Ch 1: LDV-measurement (2 μm/V). Ch 2: VCM-driver input. Ch 3: PZT-control signal.

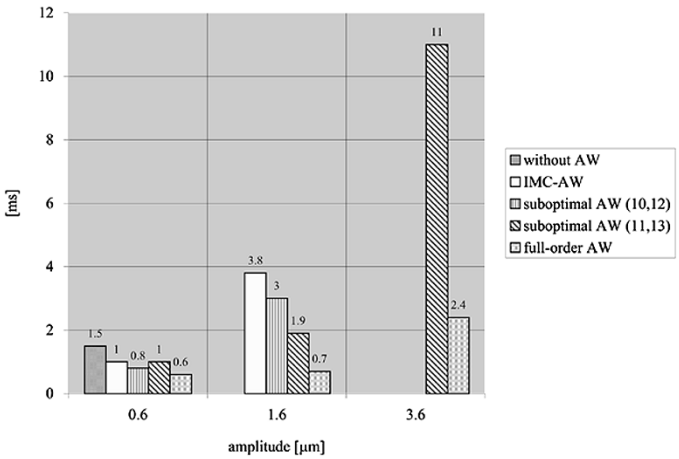

Fig. 16. Settling time t_s for different step demand amplitudes for different AW-compensator configurations.

system de-stabilising with large enough PZT-signal saturation but before VCM-actuator saturation.

For step inputs, it was observed experimentally, that the full-order AW-compensator yielded, in its whole stability region of demand magnitudes below 4 μm, performance superior to both the IMC-type and the lower order suboptimal AW-compensators. From Fig. 16 and Table III, note that the full-order compensator always gives the fastest step response settling times and the shortest times needed to recover from saturation.

Performance of the suboptimal AW-compensator is superior to the IMC-compensator in terms of saturation recovery times and settling times for steps above 1.6 μm (Fig. 16 and Table III). One of the interesting features of the suboptimal solution is its similarity with the IMC solution for *small demand amplitudes*. Both AW schemes, the suboptimal and the IMC-type scheme show some larger high-frequency oscillations in the settling process in comparison to the full order AW-scheme. It can be shown using simulation tests that these oscillations can be mainly attributed to a mismatch of the plant model used in the IMC-scheme.

Although, the suboptimal AW-scheme improves on the IMC-type scheme, as the IMC scheme is the basis for this design, some of its characteristics remain visible in the suboptimal scheme. In particular for large step demand, the slow settling behavior with large low-frequency amplitude [Figs. 14(b) and 15] is reminiscent of the IMC-AW scheme. For this, note from the equivalent AW-scheme of Fig. 4 that the nonlinear loop directly affects the disturbance output filter, which is for the IMC-case a copy of the plant model. This fact is particularly noticeable for the IMC AW case ($M = I$), once the VCM-actuator signal saturates for large step demand. In this case, the double integrator feature of the VCM-actuator will introduce the slow settling behavior (see Fig. 6 for the VCM-characteristics).

VIII. CONCLUSION

Two novel AW schemes, a suboptimal and a full order AW scheme, have been tested experimentally on a dual-stage HDD-servo system showing that the full-order AW scheme provides better results than the other tested schemes while the suboptimal AW-scheme performs better for large step demand than the IMC-type scheme.

Numerical test results have shown that shock disturbances do not destabilize the controller with AW-compensation, which contrasts the case of linear control without AW-compensation. In practice, similar results are to be expected showing significantly higher robustness of the controller with AW-compensation than without.

Although the design procedure for the sub-optimal AW compensator is the most complex, it has the ultimate merit that the AW compensator is of lower order than the full-order compensator and potentially better performing than the IMC-based AW scheme. In fact, from a certain perspective, we have been led to an AW solution similar to that discussed in [24] in that our AW compensator is a combination of the plant model (in our case a reduced-order one) and another term which acts at the controller

output - in our case a low pass filter. The design of this AW compensator was particularly challenging due to the high degree of uncertainty present in the system, the high order of the plants studied and the subsequent problem of aliasing.

More research needs to be conducted into how performance can be improved while retaining the desirable property of *large-signal* stability.

APPENDIX

If the plant and controller state-space realizations are given by

$$[G_1\ G_2] \sim \left[\begin{array}{c|cc} A_p & B_{\rm pd} & B_p \\ \hline C_p & D_{\rm pd} & D_p \end{array}\right]$$
$$[K_1\ K_2] \sim \left[\begin{array}{c|cc} A_c & B_{\rm cr} & B_c \\ \hline C_c & D_{\rm cr} & D_c \end{array}\right]$$

and the filter realizations are given by

$$F_1 \sim \left[\begin{array}{c|c} A_1 & B_1 \\ \hline C_1 & D_1 \end{array}\right], \quad F_2 = \hat{G}_2 \sim \left[\begin{array}{c|c} A_2 & B_2 \\ \hline C_2 & D_2 \end{array}\right]$$

then the constant matrices used in the LMI (5) are given by

$$\bar{A} = \begin{bmatrix} A_{11} & A_{12} & -B_{12}C_2 & B_{11}C_1 \\ A_{21} & A_{22} & -B_{22}C_2 & B_{21}C_1 \\ 0 & 0 & A_2 & 0 \\ 0 & 0 & 0 & A_1 \end{bmatrix}$$
$$\bar{B} = \begin{bmatrix} B_{11}D_1 & -B_{12}D_2 \\ B_{21}D_1 & -B_{22}D_2 \\ 0 & B_2 \\ B_1 & 0 \end{bmatrix}, \quad B_0 = \begin{bmatrix} B_{11} \\ B_{21} \\ 0 \\ 0 \end{bmatrix}$$
$$\bar{C}_1 = [C_{11} \quad C_{12} \quad -D_{12}C_2 \quad D_{11}C_1], \quad D_{01} = D_{11} - I$$
$$\bar{C}_2 = [C_{21} \quad C_{22} \quad -D_{22}C_2 \quad D_{21}C_1], \quad D_{02} = D_{21}$$
$$\bar{D}_1 = [D_{11}D_1 \quad -D_{12}D_2], \quad \bar{D}_2 = [D_{21}D_1 \quad -D_{22}D_2]$$

where

$$\begin{bmatrix} A_{11} & A_{12} \\ A_{21} & A_{22} \end{bmatrix} := \begin{bmatrix} A_p + B_p\tilde{\Delta}D_cC_p & B_p\tilde{\Delta}C_C \\ B_c\Delta C_p & A_c + B_c\Delta D_pC_c \end{bmatrix}$$
$$\begin{bmatrix} B_{11} & B_{12} \\ B_{21} & B_{22} \end{bmatrix} := \begin{bmatrix} B_p\tilde{\Delta} & B_p\tilde{\Delta}D_c \\ B_c\Delta D_p & B_c\Delta \end{bmatrix}$$
$$\begin{bmatrix} C_{11} & C_{12} \\ C_{21} & C_{22} \end{bmatrix} := \begin{bmatrix} \tilde{\Delta}D_cC_p & \tilde{\Delta}C_c \\ \Delta C_p & \Delta D_pC_c \end{bmatrix}$$
$$\begin{bmatrix} D_{11} & D_{12} \\ D_{21} & D_{22} \end{bmatrix} := \begin{bmatrix} I + \tilde{\Delta}D_cD_p & \tilde{\Delta}D_c \\ \Delta D_p & \Delta D_pD_c \end{bmatrix}.$$

ACKNOWLEDGMENT

The authors are grateful to A. Tan, N. Suriadi, and T. Hong Yip from the A*STAR Data Storage Institute, Singapore, for their invaluable and unconditional help and support.

REFERENCES

[1] B. M. Chen, T. H. Lee, K. Peng, and V. Venkataramanan, "Composite nonlinear feedback control for linear systems with input saturation: Theory and an application," *IEEE Trans. Automat. Contr.*, vol. 48, pp. 427–439, Mar. 2003.

[2] K. K. Chew, "4-d shock-sensing for hard-disk drives," *IEEE Trans. Magn.*, vol. 35, pp. 2487–2489, Dec. 1999.

[3] C. Du, J. Zhang, and G. Guo, "Vibration analysis and control design comparison of HDD's using fluid bearing and ball bearing spindles," in *Proc. 2001 Amer. Contr. Conf.*, vol. 2, 2001, pp. 1378–1383.

[4] C. Edwards and I. Postlethwaite, "Anti-windup and bumpless transfer schemes," *Automatica*, vol. 34, no. 2, pp. 199–210, 1998.

[5] G. Grimm, J. Hatfield, I. Postlethwaite, A. R. Teel, M. C. Turner, and L. Zaccarian, "Antiwindup for stable linear systems with input saturation: An LMI based synthesis," *IEEE Trans. Automat. Contr.*, vol. 48, pp. 1509–1525, Sept. 2003.

[6] G. Grimm, I. Postlethwaite, A. R. Teel, M. C. Turner, and L. Zaccarian, "Case studies using linear matrix inequalities for optimal anti-windup compensator synthesis," in *Proc. Eur. Control Conf.*, 2001.

[7] ——, "Linear matrix inequalities for full and reduced order anti-windup synthesis," in *Proc. American Control Conf.*, 2001.

[8] G. Guo, D. Wu, and T. C. Chong, Modified dual-stage conbtroller for dealing with secondary stage actuator saturation, in IEEE Trans. Magnetics, 2003, to be published.

[9] R. Hanus, M. Kinnaert, and J. L. Henrotte, "Conditioning technique, a general anti-windup and bumpless transfer method," *Automatica*, vol. 23, pp. 729–739, 1987.

[10] J. L. Herrmann and G. Guo, "HDD dual-stage servo-controller design using a μ-analysis tool," *Control Engineering Practice*, to be published.

[11] Y. Huang, M. Banther, P. D. Mathur, and W. C. Messner, "Design and analysis of a high bandwidth disk drive servo-system using an instrumented suspension," *IEEE Trans. Mechatron.*, vol. 4, pp. 196–206, Feb. 1999.

[12] M. Kobayashi and R. Horowitz, "Track seeking control for hard disc dual-stage servo systems," *IEEE Trans. Magn.*, vol. 37, pp. 949–954, Feb. 2001.

[13] M. Kobayashi, S. Nakagawa, T. Atsumi, and T. Yamaguchi, "High-bandwidth servo control designs for magnetic disc drives," in *Proc. IEEE Int. Conf. Advanced Intelligent Mechatronics*, Como, Italy, 2001, pp. 1124–1129.

[14] X. Liu, A. Li, W. Clegg, D. Jenkins, and P. Davey, "Head disk spacing variation suppresion via active flying height control," in *Proc. IEEE Instr. and Meas. Techn. Conf.*, Budapest, Hungary, 2001, pp. 888–891.

[15] Y. Lou, P. Gao, B. Qin, G. Guo, E. H. Ong, A. Takada, and K. Okada, "Dual-stage servo with on-slider PZT microactuator for hard disk drives," *IEEE Trans. Magn.*, vol. 38, pp. 2183–2185, Dec. 2002.

[16] K. Mori, T. Munemoto, H. Otsuki, Y. Yamaguchi, and K. Akagi, "A dual-stage magnetic disk drive actuator using a piezoelectric device for high track density," *IEEE Trans. Magn.*, vol. 27, pp. 5298–5300, Dec. 1991.

[17] E. F. Mulder and M. V. Kothare, "Synthesis of stabilising anti-windup controllers using piecewise quadratic Lyapunov functions," in *Proc. American Control Conf.*, 2000, pp. 3239–3243.

[18] E. F. Mulder, M. V. Kothare, and M. Morari, "Multivariable anti-windup controller synthesis using linear matrix inequalities," *Automatica*, vol. 37, pp. 1407–1416, 2000.

[19] S. Nakagawa, T. Yamaguchi, H. Numasato, H. Hosokawa, and H. Hirai, "Improving the disturbance resistance of magnetic disk drives by using anti-windup and model following controls with initial value compensation," *JSME Int. J.*, ser. C, vol. 43, no. 3, pp. 618–624, 2000.

[20] H. Numasato and M. Tomizuka, "Settling control and performance of dual-actuator system for hard disk drives," in *Proc. 2001 American Control Conf.*, vol. 4, 2001, pp. 2779–2785.

[21] R. Oboe, "MEMS-based accelerometers use in hard disk drives," *Micro. Technol.*, vol. 8, pp. 174–181, 2002.

[22] S. J. Schroeck, W. C. Messner, and R. J. McNab, "On compensator design for linear time-invariant dual-input single-output systems," *IEEE Trans. Mechatron.*, vol. 6, pp. 50–57, Feb. 2001.

[23] T. Semba, "An H_∞ design method for a multi-rate servo controller and applications to a high density hard disk drive," in *Proc. IEEE Conf. Dec. Control*, Orlando, FL, 2001, pp. 2219–2221.

[24] A. R. Teel and N. Kapoor, "The $\mathcal{L}_2$ anti-windup problem: Its definition and solution," in *Proc. Eur. Control Conf.*, 1997.

[25] M. Tokuyama, T. Shimizu, H. Masuda, S. Nakamura, M. Hanya, O. Iriuchijima, and J. Soga, "Development of a ϕ-shaped actuated suspension for 100-ktpi hard disk drives," *IEEE Trans. Magn.*, vol. 37, pp. 1884–1886, Dec 2001.

[26] M. C. Turner, I. Postlethwaite, and D. J. Walker, "Non-linear tracking control for multivariable constrained input linear systems," *Int. J. Contr.*, vol. 73, no. 12, pp. 1160–1172, 2000.

[27] M. C. Turner and I. Postlethwaite, "Robustness analysis of general conditioning schemes for stable systems," in *Proc. Workshop Systems Time Domain Constraints*, 2000.

[28] ——, A new perspective on static and low order anti-windup synthesis, in Int. J. Control, 2003. accepted, submitted for publication.
[29] ——, "Discrete-time anti-windup synthesis," Dept. Eng, Univ. Leicester, Tech. Rep., 2001.
[30] V. Venkataramanan, K. Peng, B. M. Chen, and T. H. Lee, "Discrete-time composite nonlinear feedback control with an application in design of a hard disk drive servo system," *IEEE Trans. Contr. Syst. Technol.*, vol. 11, pp. 16–23, Jan. 2003.
[31] K. S. Walgama, S. Ronnback, B. M. Chen, and J. Sternby, "Generalization of the conditioning technique for anti-windup compensators," in *Inst. Elect. Eng. Part D*, vol. 139, 1992, pp. 109–118.
[32] P. F. Weston and I. Postlethwaite, "Analysis and design of linear conditioning schemes for systems containing saturating actuators," in *Proc. IFAC Nonlinear Control System Design Symp.*, 1998.
[33] L. Yi and M. Tomizuka, "Two-degree-of-freedom control with robust feedback control for hard disk servo systems," *IEEE Trans. Mechatron.*, vol. 4, pp. 17–24, Mar. 1999.
[34] K. Zhou, J. C. Doyle, and K. Glover, *Robust and Optimal Control*. Englewood Cliffs, NJ: Prentice-Hall, 1996.

Guido Herrmann (M'99) was born in Berlin, Germany, in 1972. He received the Diplom-Ingenieur der Elektrotechnik degree (with highest honors) from the Technische Universität zu Berlin, Germany, and the Ph.D. degree, sponsored by the Daimler-Benz-Foundation, Germany, and by a Marie-Curie Fellowship, from the University of Leicester, Leicester, U.K., in 1997 and 2001, respectively.

From 2001 to 2003, he was a Senior Research Fellow at the A*STAR Data Storage Institute, Singapore. In 2003, he joined the University of Leicester. His research interests are in the theory and application of nonlinear and robust control in particular sampled-data, anti-windup, sliding-mode, and NN-control, as well as regulation of chaotic systems.

Matthew C. Turner (M'99) was born in Corby, U.K., in 1975. He received the B.Eng. degree in electrical and electronic engineering, from the University of Surrey, Surrey, U.K., in 1996, and the Ph.D. in control engineering from the University of Leicester, Leicester, U.K., in 2000.

His main research interests are centered around robust control, flight control and the control of systems containing isolated nonlinearities. He has designed and implemented robust controllers and anti-windup compensators on several industrial engineering systems and is currently involved with the European aerospace group, GARTEUR, in investigating the phenomenon of pilot-induced-oscillations.

Dr. Turner is a member of the Institute for Electrical Engineers (IEE), U.K.

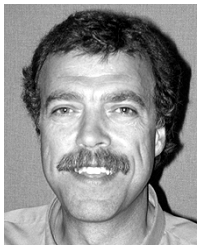

Ian Postlethwaite (M'79–SM'92–F'01) was born in Wigan, U.K., in 1953. He received a First Class B.Sc. (Eng.) degree from Imperial College, London University, U.K., in 1975 and the Ph.D. degree from Cambridge University, Cambridge, U.K., in 1978.

From 1978 to 1981, he was a Research Fellow at Cambridge University and spent six months at the General Electric Company, Schenectady, NY. In 1981, he was appointed to a Lectureship with the Engineering Science Department at Oxford University, U.K., and in 1988 he moved to a Chair of Engineering at the University of Leicester where he is now Head of Department. He has held short visiting positions at the University of California at Berkeley, at the University of California at Santa Barbara, at the Australian National University, Canberra, and at the University of Auckland, Auckland, New Zealand. He is a co-author of *Multivariable Feedback Control* (New York, Wiley, 1996). His research involves theoretical contributions to the field of robust multivariable control and the application of advanced control system design to engineering systems.

Dr. Postlethwaite is a Fellow of the Institute for Electrical Engineers (IEE), U.K. and the InstMC. In 1991, he received the IEE FC Williams premium; in 2001, he was awarded the Sir Harold Hartley Medal of the InstMC; and in 2002, he received a Best Paper Prize from the IFAC Journal of Control Engineering Practice.

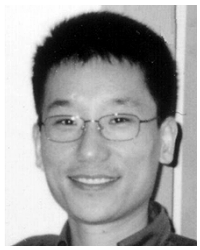

Guoxiao Guo (S'95–M'96) received the B.Eng. and M.Eng. degrees from Tsinghua University, Beijing, China, in 1989 and 1994, respectively, and the Ph.D. degree in electrical engineering from Nanyang Technological University, Singapore, in1997.

He joined the A*STAR Data Storage Institute, Singapore, in 1995. Currently, he is the Manager of the Mechatronics and Recording Channel Division. He is also an Adjunct Fellow at the National University of Singapore. His research interests include nonlinear and robust control, mechatronics and MEMS, vibration analysis and control, with application to nano positioning systems.